

# High-Fidelity, Adaptive Qubit Measurements through Repetitive Information Transfer

D. B. Hume, T. Rosenband and D. J. Wineland

Time and Frequency Division, National Institute of Standards and Technology, 325 Broadway, Boulder, Colorado 80305, USA

Using two trapped ion species ( $^{27}\text{Al}^+$  and  $^9\text{Be}^+$ ) as primary and ancillary systems, we implement qubit measurements based on the repetitive transfer of information and quantum nondemolition detection. The repetition provides a natural mechanism for an adaptive measurement strategy, which leads to exponentially lower error rates compared to using a fixed number of detection cycles. For a single qubit we demonstrate 99.94 % measurement fidelity. We also demonstrate a technique for adaptively measuring multiple qubit states using a single ancilla, and apply the technique to spectroscopy of an optical clock transition.

PACS numbers: 03.67.-a

Reliable state detection plays a central role in quantum-limited metrology and quantum information processing. For example, in quantum computation, low error probabilities during detection are required to achieve good efficiency [1]. In practice, detection fidelity is limited by state perturbations and noise during the measurement process. One way to mitigate these effects is to couple the primary quantum system to an ancillary quantum system used for measurement [1, 2, 3, 4, 5]. If the measurement process does not affect the projected states of the primary system, it constitutes a quantum non-demolition (QND) measurement [5, 6, 7, 8, 9]. An important feature of a QND measurement is its repeatability, which allows for high fidelity state detection in the presence of noise. The repetitive transfer of information from the primary to the ancillary system followed by detection of the ancilla state provides a natural mechanism for real-time measurement feedback, which can further enhance detection efficiency [10, 11].

Ancilla-assisted detection, as formulated here, follows three steps: (1) ancilla preparation, (2) coupling the ancilla and primary systems, and (3) ancilla measurement. These steps are described by a quantum-mechanical operator  $\hat{H}(t)$ , which includes the free evolution of the states as well as the interactions necessary for measurement. If this operator commutes with the measured observable of the primary system,  $\hat{O}_P$ , that is if

$$[\hat{H}(t), \hat{O}_P] = 0, \quad (1)$$

for all  $t$ , then it is a QND measurement [2, 6]. As an example, consider measuring a single qubit in the superposition state  $\alpha|\downarrow\rangle_P + \beta|\uparrow\rangle_P$ , and let  $\hat{O}_P = |\downarrow\rangle_P\langle\downarrow|_P$  so that  $\langle\hat{O}_P\rangle = |\alpha|^2$ . The ancilla is first prepared in a known initial state,  $|\downarrow\rangle_A$ . During subsequent interaction with the primary system the state evolves to

$$\alpha|\downarrow\rangle_P|\downarrow\rangle_A + \beta|\uparrow\rangle_P|\uparrow\rangle_A. \quad (2)$$

The state of the coupled system is now detected by applying the measurement operator for the ancillary system,  $\hat{O}_A = |\downarrow\rangle_A\langle\downarrow|_A$ . In this ideal case,

$$\langle\hat{O}_A\rangle = \langle\hat{O}_P\rangle. \quad (3)$$

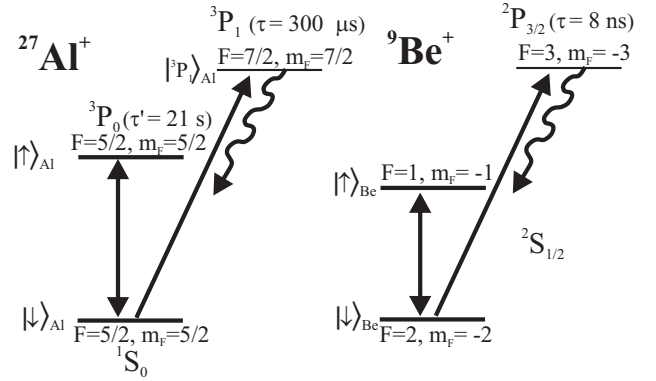


FIG. 1: Relevant energy levels in  $\text{Al}^+$  and  $\text{Be}^+$ . The states  $|\downarrow\rangle_{\text{Al}}$  and  $|\uparrow\rangle_{\text{Al}}$  form the qubit to be measured. The  $m_F = \frac{7}{2}$  Zeeman sublevel of the  $^3P_1$  state forms a closed transition with  $|\downarrow\rangle_{\text{Al}}$ . The widely separated excited state lifetimes in  $\text{Al}^+$ , 21 s and 300  $\mu\text{s}$ , allow for many repetitions of the detection procedure in a single experiment. The qubit states in  $\text{Be}^+$  are distinguished by state-dependent resonance fluorescence [12].

In the presence of noisy interactions and imperfect ancilla measurements, Eq. (3) is not strictly upheld. But, to the degree that Eq. (1) holds and the measurement constitutes a QND measurement, it may be repeated several times to improve the measurement fidelity. The aggregate detection after multiple cycles of information transfer and ancilla measurement projects the primary quantum system into the state  $|\downarrow\rangle_P(|\uparrow\rangle_P)$  with probability  $|\alpha|^2$  ( $|\beta|^2$ ). Multiple detection cycles also allow for the measurement of multiple-qubit states by use of a single ancilla. By altering the conditions of interaction between the primary and ancillary systems the measurement can be chosen to discriminate different sets of eigenstates [2].

We apply these ideas to high-fidelity measurements of one and two-qubit systems in an ion trap. We employ two ion species,  $^{27}\text{Al}^+$  and  $^9\text{Be}^+$ , trapped in the same harmonic well. The  $\text{Al}^+$  ions form the primary quantum system and a single  $\text{Be}^+$  ancilla is used for sympathetic laser cooling [13] and state detection [4]. Both ion species can be considered as qubits, each

having an auxiliary internal state used in the detection procedure (Fig. 1). In  $\text{Al}^+$ , the qubit states consist of the  $|^1S_0; F = \frac{5}{2}, m_F = \frac{5}{2}\rangle \equiv |\downarrow\rangle_{\text{Al}}$  ground state and the metastable  $|^3P_0; F = \frac{5}{2}, m_F = \frac{5}{2}\rangle \equiv |\uparrow\rangle_{\text{Al}}$  optically excited state. Transitions through the  $|^3P_1; F = \frac{7}{2}, m_F = \frac{7}{2}\rangle \equiv |^3P_1\rangle_{\text{Al}}$  auxiliary state mediate the measurement interaction. In  $\text{Be}^+$ , two hyperfine Zeeman sublevels of the  $^2S_{1/2}$  ground state,  $|F = 2, m_F = -2\rangle \equiv |\downarrow\rangle_{\text{Be}}$  and  $|F = 1, m_F = -1\rangle \equiv |\uparrow\rangle_{\text{Be}}$ , comprise the qubit. A pair of laser beams induces coherent stimulated-Raman transitions between  $\text{Be}^+$  qubit states. Detection of the  $\text{Be}^+$  state relies on state-dependent resonance fluorescence from the  $|\downarrow\rangle_{\text{Be}} \rightarrow |^2P_{3/2}; F = 3, m_F = -3\rangle$  cycling transition[12].

Before measurement the  $\text{Al}^+$  system is prepared in a superposition state. The ions are then laser-cooled to the motional ground state[13] and  $\text{Be}^+$  is initialized to  $|\downarrow\rangle_{\text{Be}}$ [12]. A series of laser pulses transfers the information in the  $\text{Al}^+$  system first to the collective motional state then to the  $\text{Be}^+$  internal state followed by  $\text{Be}^+$  detection. The individual steps and their durations are:

1. Doppler cooling all modes ( $\simeq 600 \mu\text{s}$ )
2. Raman cooling axial modes to ground state (1 ms)
3.  $\text{Be}^+$  preparation to the state  $|\downarrow\rangle_{\text{Be}}$  (1  $\mu\text{s}$ )
4. Interaction between  $\text{Al}^+$  and  $\text{Be}^+$  ( $\simeq 25 \mu\text{s}$ )
5.  $\text{Be}^+$  state detection (200  $\mu\text{s}$ )

The procedure for generating the interaction of step 4 depends on the number of  $\text{Al}^+$  ions to be measured and the ion configuration. To measure the state of one  $\text{Al}^+$  we couple the ions through the axial in-phase motional mode ( $\omega_m = 2\pi \times 2.62 \text{ MHz}$ )[4]. Here, we denote Fock states of motion as  $|n\rangle_m$ . First, a  $\pi$ -pulse on the  $|\downarrow\rangle_{\text{Al}}|0\rangle_m \rightarrow |^3P_1\rangle_{\text{Al}}|1\rangle_m$  sideband transition inserts a motional quantum into the mode dependent on the ion being in the  $|\downarrow\rangle_{\text{Al}}$  state. The information in the motional state is then transferred to the internal state of  $\text{Be}^+$  using a  $\pi$ -pulse on the  $|\downarrow\rangle_{\text{Be}}|1\rangle_m \rightarrow |\uparrow\rangle_{\text{Be}}|0\rangle_m$  transition. This sequence implements an entangling operation,

$$(\alpha|\downarrow\rangle_{\text{Al}} + \beta|\uparrow\rangle_{\text{Al}})|\downarrow\rangle_{\text{Be}} \rightarrow \alpha|^3P_1\rangle_{\text{Al}}|\uparrow\rangle_{\text{Be}} + \beta|\uparrow\rangle_{\text{Al}}|\downarrow\rangle_{\text{Be}}, \quad (4)$$

leaving the system in a state analogous to that of Eq (2). After measurement, the  $\text{Al}^+$  ion is projected into  $|\uparrow\rangle_{\text{Al}}$  with probability  $|\beta|^2$ . Because the  $^1S_0$  to  $^3P_1$  transition is closed, the  $\text{Al}^+$  ion is projected into the manifold of  $|\downarrow\rangle_{\text{Al}}$  and  $|^3P_1\rangle_{\text{Al}}$  states with probability  $|\alpha|^2$ . Although temporary optical excitation into  $|^3P_1\rangle_{\text{Al}}$  represents a departure from the strict definition of a QND measurement, we can formally address this by defining the state  $|\downarrow\rangle_{\text{Al}}$  to include the eigenspace spanned by the  $^1S_0$  and  $^3P_1$  states. In any case, spontaneous emission from the  $^3P_1$  state ( $\tau \simeq 300 \mu\text{s}$ ) effectively re-prepares  $\text{Al}^+$  back in  $|\downarrow\rangle_{\text{Al}}$  with probability greater than 99 % before another detection cycle can be implemented.

Imperfect cooling and transfer pulses give rise to a single-cycle detection error of approximately 15 %. How-

ever, the fidelity can be improved by repeating the procedure. For the  $j$ th cycle of the measurement procedure, a number of photons  $n_j$  is scattered from the  $\text{Be}^+$  ion and collected in a photomultiplier tube. The entire measurement yields a series of photon counts,  $\{n_j\}$ , that are used to determine the  $\text{Al}^+$  state. Here, we use a computer to analyze  $n_j$  in real-time, providing the means to actively control the measurement process. Before the first cycle, we assume equal prior likelihoods for  $\text{Al}^+$  states. The probability,  $P(n|i)$ , of observing  $n$  photons given state  $|i\rangle$  of the  $\text{Al}^+$  system is determined based on histograms continuously updated from previous measurements[14]. The probability,  $P(\{n_j\}|i)$ , of  $|i\rangle$  producing the observed series of photon counts is  $P(\{n_j\}|i) = \prod_j P(n_j|i)$ . Applying Bayes' rule,

$$P(i|\{n_j\}) = \frac{P(\{n_j\}|i)}{\sum_k P(\{n_j\}|k)}, \quad (5)$$

yields the probability of a particular state  $|i\rangle$  given the observed series of photon counts. Here,  $k$  spans all states in the  $\text{Al}^+$  system, for example the two qubit states in the case of a single aluminum ion. This procedure provides both the most likely state of  $\text{Al}^+$ ,  $|i_{\text{max}}\rangle$ , and also the probability of measurement error,  $1 - P(i_{\text{max}}|\{n_j\})$ . The first assigns detection outcomes, while the second is used to optimize the measurement process. Specifically, we repeat the detection cycles only until the aggregate detection reaches a desired error probability.

To experimentally determine the error rate for state discrimination, we compare two consecutive detection sequences, each of which separately determines  $|i\rangle$  and reaches a specified minimum error probability. If the two results agree, both detections are counted as correct, while disagreement signifies an error. This analysis allows us to compare the actual error rate with the real-time prediction. Errors quantified in this way also represent the fidelity of quantum state preparation[15]. The results for a single  $\text{Al}^+$  ion are plotted in Fig. 2. The observed errors agree well with the predicted error rate for fidelities up to 99.94 %. In the case of detecting  $|\downarrow\rangle_{\text{Al}}$ , the observed error rate is as low as  $9 \times 10^{-5}$ . However,  $|\uparrow\rangle_{\text{Al}}$  detections, the state lifetime of 21 s limits the number of times the detection cycle can be repeated and still yield an accurate prediction. Here, the observed error rate reaches a minimum at  $6 \times 10^{-4}$ , then increases to above  $1 \times 10^{-3}$  as we demand higher measurement confidence through more repetitions. This error rate agrees with that predicted from the decay rate and the interval between detection cycles. The  $|\uparrow\rangle_{\text{Al}}$  state lifetime  $\tau'$  and measurement cycle duration,  $t_c$  set an upper bound on the attainable detection fidelity; that is, no measurement can achieve an error rate lower than the probability of decay before the first detection,  $t_c/\tau' \simeq 10^{-4}$  in the experiment here.

To demonstrate the gain in sensitivity achieved with adaptive measurements, we perform a Monte-Carlo simulation of the detection procedure based on experimentally observed histograms. We compare the adaptive

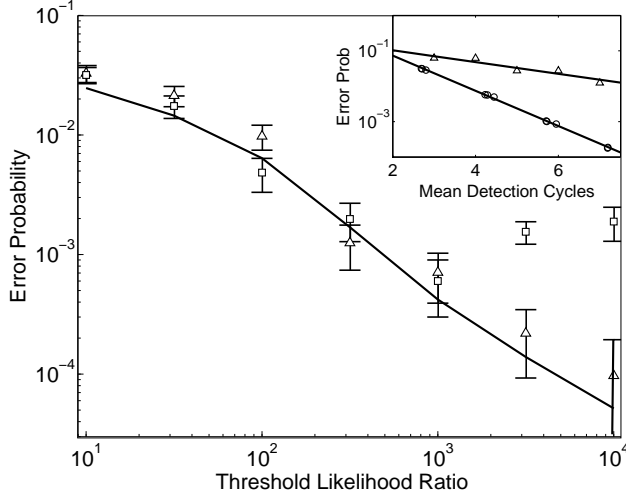


FIG. 2: Observed (symbols) and calculated (solid line) error rates for repeated detections are plotted as a function of the threshold likelihood ratio defined as the greater of  $P(\{n_j\}|\uparrow)_{Al}/P(\{n_j\}|\downarrow)_{Al}$  or  $P(\{n_j\}|\downarrow)_{Al}/P(\{n_j\}|\uparrow)_{Al}$ . Once the likelihood ratio exceeds the threshold value, detection is stopped. The  $^1S_0$  detections (triangles) reach a repeatability of 99.99 % while  $^3P_0$  detections (squares) are limited by the state lifetime to 99.94 %. This is achieved for a desired likelihood ratio of  $10^3$ , requiring a mean number of detection cycles equal to 6.54. Inset: Simulation of qubit detection, using experimental histograms, comparing the case in which the number of detection cycles is fixed (diamonds) to that in which it is adaptive (circles). The ability to estimate errors in real time gives rise to an exponentially lower error rate as a function of time.

scheme, which uses the minimum number of cycles necessary to achieve a given fidelity, to a detection scheme where the number of detection cycles is set to a particular value [Fig. 2(inset)]. As a function of average detection duration, the adaptive detection gives an exponentially smaller error rate. In both simulations the final state determination results from Bayesian analysis, which gives optimal results based on the detection record. Thus, in the case of fixed detections, the plotted error rate provides a lower bound for the infidelity of commonly used fixed detection strategies such as majority vote.

Adaptive detection also provides a means to measure and prepare the state of a multiple qubit system without the need for individual qubit addressing. Although a single ancilla qubit can yield at best one bit of information in a measurement cycle, repeating the measurement process and varying the parameters of the interaction yields more information[2]. To demonstrate the detection of two  $Al^+$  ions, we use a symmetric spatial configuration of the ions ( $Be^+$  centered between the two  $Al^+$  ions). First, all nine normal modes are Doppler cooled. The antisymmetric modes, which normally don't couple to  $Be^+$ , are Doppler cooled sympathetically by first distorting the ion configuration with application of a static field and then

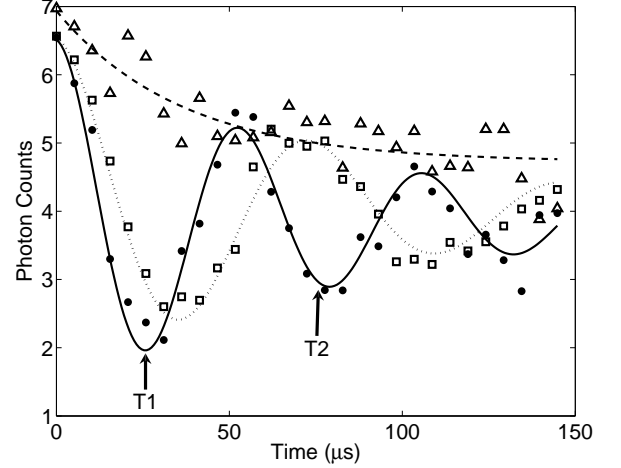


FIG. 3: Red sideband Rabi flopping on the  $|\downarrow\rangle_{Al} - |^3P_1\rangle_{Al}$  transition beginning with one quantum of motion. The fluorescence signal is obtained after transferring the motional information to the qubit state of  $Be^+$ . The three possible numbers of aluminum ions in the ground state, 2 (solid circles), 1 (empty squares), and 0 (empty triangles), are distinguished by their sideband Rabi rate. For zero ground state ions, the known signal admixture from one ground state ion due to detection errors was removed. We determine the state of excitation in the aluminum ion system after making multiple mapping sequences with pulses of duration T1 or T2.

adiabatically relaxing the system back to the aligned configuration. The two axial modes that couple to  $Be^+$  are cooled to the ground state and  $Be^+$  is prepared in  $|\downarrow\rangle_{Be}$ .

The measurement interaction for two  $Al^+$  ions proceeds as follows:

1.  $Be^+$ :  $|\downarrow\rangle_{Be}|0\rangle_m \rightarrow |\uparrow\rangle_{Be}|1\rangle_m$  ( $T_\pi$ ).
2.  $Al^+$ :  $|\downarrow\rangle_{Al}|1\rangle_m \rightarrow |^3P_1\rangle_{Al}|0\rangle_m$  ( $T_{var}$ ).
3.  $Be^+$ :  $|\uparrow\rangle_{Be}|1\rangle_m \rightarrow |\downarrow\rangle_{Be}|0\rangle_m$  ( $T_\pi$ ).

where  $T_\pi$  is the sideband  $\pi$ -time for the  $Be^+$  qubit transition and  $T_{var}$  is a variable duration. The first pulse inserts a quantum of motion into the selected motional mode, the second pulse entangles the motional state with the internal  $Al^+$  qubit pair, and the final pulse transfers information in the motional state to the internal state of  $Be^+$ .

The  $^3P_1$  sideband Rabi rate (step 2) depends only on the number of  $|\downarrow\rangle_{Al}$  ions (zero, one or two). Experimental excitation curves for these three cases are plotted in Fig. 3. With one  $Al^+$  ion in  $|\downarrow\rangle_{Al}$ , flopping between  $|\downarrow\rangle_{Al}|1\rangle_m$  and  $|^3P_1\rangle_{Al}|0\rangle_m$  will proceed with a Rabi rate given by  $\Omega_{R,1} \simeq \Omega_c\eta$ , where  $\Omega_c$  is the carrier Rabi frequency and  $\eta$  is the Lamb-Dicke parameter for the aluminum ions[12]. With two  $Al^+$  ions in  $|\downarrow\rangle_{Al}$ , Rabi flopping carries the aluminum system to an entangled state,  $|\downarrow\rangle_{Al}|\downarrow\rangle_{Al}|1\rangle_m \rightarrow \frac{1}{\sqrt{2}}(|^3P_1\rangle|\downarrow\rangle_{Al} + |\downarrow\rangle_{Al}|^3P_1\rangle)|0\rangle_m$  with characteristic Rabi rate  $\Omega_{R,2} \simeq \sqrt{2}\Omega_c\eta$ [16]. The fitted Rabi rates agree with those expected.

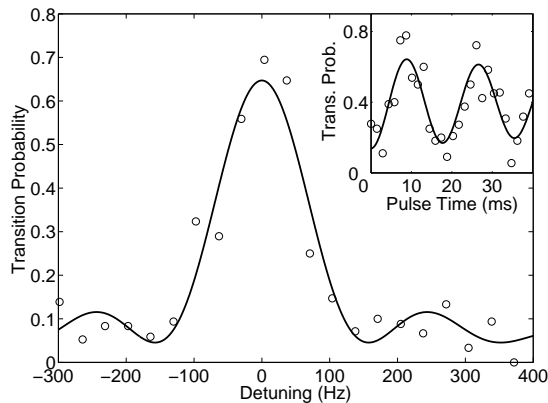


FIG. 4: Signal from  $^3P_0$  spectroscopy using two  $\text{Al}^+$  and one  $\text{Be}^+$  ancilla. Obtaining this signal depends on the ability to prepare the  $|\downarrow\rangle_{\text{Al}}|\downarrow\rangle_{\text{Al}}$  or  $|\uparrow\rangle_{\text{Al}}|\uparrow\rangle_{\text{Al}}$  state of the  $\text{Al}^+$  system because transitions between  $|\downarrow\rangle_{\text{Al}}|\uparrow\rangle_{\text{Al}}$  and  $|\uparrow\rangle_{\text{Al}}|\downarrow\rangle_{\text{Al}}$  will not be detected. Inset: Rabi flopping on the  $^3P_0$  transition. Signal contrast is limited by fluctuations in the transition excitation, rather than detection efficiency.

Two particular transfer pulse durations,  $T_1 = 30 \mu\text{s}$  and  $T_2 = 80 \mu\text{s}$ , exhibit good discrimination between one particular state and the other two. A combination of detection cycles using these two pulse durations distinguishes the three states. In this scheme, the maximum likelihood analysis plays the additional role of determining which pulse duration to use based on previous measurements. The duration is chosen to maximize contrast

between the two most-likely states of the aluminum system.

We have performed spectroscopy of the  $|\downarrow\rangle_{\text{Al}} \rightarrow |\uparrow\rangle_{\text{Al}}$  transition on two  $\text{Al}^+$  ions using this scheme. Figure 4 shows a Fourier-limited lineshape and Rabi flopping (inset). Various sources of noise including ion temperature, laser intensity noise and off-resonant excitation of the ground state into the  $^3P_1, F = \frac{7}{2}, m_F = \frac{5}{2}$  state due to imperfect polarization are the primary limits to signal contrast. As before, we measure the error rate for state discrimination by comparing consecutive detection sequences, and find a detection fidelity of 98.3%. Improvements in laser cooling could improve signal contrast and detection fidelity.

A practical application for the techniques we describe is the operation of an optical atomic clock based on  $\text{Al}^+$  [17]. The time scale for probing the  $^1S_0 \rightarrow ^3P_0$  transition (100 ms) significantly exceeds the detection duration ( $\simeq 10$  ms) so that the clock performance is not significantly affected by the detection duration. These techniques may also be important for scalable quantum computation. Efficient state detection is a basic requirement, which may ultimately depend on repeated QND measurements as demonstrated here. More specifically, trapped ion systems composed of two species have previously been proposed for large-scale QIP [18, 19]. Here, one species carries the qubit, and the other provides sympathetic cooling. Such a two-species system could also utilize an analogous protocol to the one we describe, thereby reaching very high detection fidelity in a minimal time period.

- 
- [1] D. P. DiVincenzo, *Scalable Quantum Computers* (Wiley-VCH, Berlin, 2001).
  - [2] S. Haroche and J.-M. Raimond, *Exploring the Quantum* (Oxford University Press, Oxford, 2006).
  - [3] T. Schaetz et al., Phys. Rev. Lett. **94**, 010501 (2005).
  - [4] P. O. Schmidt et al., Science **309**, 749 (2005).
  - [5] S. Gleyzes et al., Nature **446**, 297 (2007).
  - [6] C. Caves et al., Rev. Mod. Phys. **52**, 341 (1980).
  - [7] S. Peil and G. Gabrielse, Phys. Rev. Lett. **83**, 1287 (1999).
  - [8] T. Meunier et al., Phys. Rev. B **74**, 195303 (2006).
  - [9] A. Lupascu et al., Nat Phys **3**, 119 (2007).
  - [10] M. A. Armen et al., Phys. Rev. Lett. **89**, 133602 (2002).
  - [11] Cook et al., Nature **446**, 774 (2007).
  - [12] C. Monroe et al., Phys. Rev. Lett. **75**, 4011 (1995).
  - [13] M. D. Barrett et al., Phys. Rev. A **68**, 042302 (2003).
  - [14] Updates are made by applying an exponential filter to previous measurement results, providing accurate histograms even if experimental parameters slowly drift.
  - [15] A. Lupascu et al., Phys. Rev. Lett. **96**, 127003 (2006).
  - [16] B. E. King et al., Phys. Rev. Lett. **81**, 1525 (1998).
  - [17] T. Rosenband et al., arXiv:physics/0703067v2 [physics.atom-ph] (2007).
  - [18] D. J. Wineland et al., J. Res. NIST **103**, 259 (1998).
  - [19] D. Kielpinski, C. Monroe, and D. J. Wineland, Nature **417**, 709 (2002).